Schneider, J. M., Rickenmann, D., Turowski, J., Schmid, B., Kirchner, J. W. (2016): Bed load transport in a very steep mountain stream (Riedbach, Switzerland): Measurement and prediction. - *Water Resources Research*, *52*, 12, pp. 9522—9541.

DOI: http://doi.org/10.1002/2016WR019308

AGU PUBLICATIONS

Water Resources Research

RESEARCH ARTICLE
10.1002/2016WR019308

Bed load transport in a very steep mountain stream (Riedbach, Switzerland): Measurement and prediction

Johannes M. Schneider [1,2], Dieter Rickenmann [1], Jens M. Turowski [1,3], Bastian Schmid [1,4], and James W. Kirchner [1,2]

[1]Mountain Hydrology and Mass Movements, Swiss Federal Research Institute WSL, Birmensdorf, Switzerland, [2]Department of Environmental Systems Science, ETH Zurich, Zurich, Switzerland, [3]Now at Helmholtz Centre Potsdam, GFZ German Research Centre for Geosciences, Potsdam, Germany, [4]Now at Niederer + Pozzi Umwelt AG, Uznach, Switzerland

Key Points:
- Fluvial bed load transport measured at bed gradients from 3% up to 38%
- Bed load transport approximately constant with increasing bed gradient
- Bed load transport equations for flat streams also apply in steep channels

Supporting Information:
- Supporting Information S1
- Data Set S1
- Data Set S2

Correspondence to:
D. Rickenmann,
dieter.rickenmann@wsl.ch

Citation:
Schneider, J. M., D. Rickenmann, J. M. Turowski, B. Schmid, and J. W. Kirchner (2016), Bed load transport in a very steep mountain stream (Riedbach, Switzerland): Measurement and prediction, *Water Resour. Res.*, *52*, 9522–9541, doi:10.1002/2016WR019308.

Received 8 JUN 2016
Accepted 15 NOV 2016
Accepted article online 18 NOV 2016
Published online 23 DEC 2016

Abstract Compared to lower-gradient channels, steep mountain streams typically have rougher beds and shallower flow depths, making macro-scale flow resistance (due to, e.g., immobile boulders and irregular bedforms) more important as controls on sediment transport. The marked differences in hydraulics, flow resistance, and grain mobility between steep and lower-gradient streams raise the question of whether the same equations can predict bed load transport rates across wide ranges of channel gradients. We studied a steep, glacier-fed mountain stream (Riedbach, Ct. Valais, Switzerland) that provides a natural experiment for exploring how stream gradients affect bed load transport rates. The streambed gradient increases over a 1 km stream reach by roughly one order of magnitude (from 3% to 38%), while flow discharge and width remain approximately constant. Sediment transport rates were determined in the 3% reach using *Bunte* bed load traps and in the 38% reach using the Swiss plate geophone system. Despite a ten-fold increase in bed gradient, bed load transport rates did not increase substantially. Observed transport rates for these two very different bed gradients could be predicted reasonably well by using a flow resistance partitioning approach to account for increasing bed roughness (D_{84} changes from 0.17 m to 0.91 m) within a fractional bed load transport equation. This suggests that sediment transport behavior across this large range of steep slopes agrees with patterns established in previous studies for both lower-gradient and steep reaches, and confirms the applicability of the flow resistance and bed load transport equations at very steep slopes.

1. Introduction

Bed load transport in steep mountain streams is an important agent in fluvial geomorphology [*Schumm*, 1977], river engineering [*Yang*, 1996] and natural hazard assessment [*Badoux et al*., 2014]. However, the processes driving bed load transport at steep slopes are still not fully understood and bed load prediction remains challenging. Direct observations of bed load transport and hydraulic conditions in these steep streams are rare, complicating model development and validation. In addition, the process understanding and predictive equations that are available for lower-gradient channels cannot be easily translated to steeper channels, because factors controlling bed load transport, such as the bed configuration and hydraulic conditions, change with the bed gradient [*Bathurst et al*., 1987].

Moving upstream from lower gradients to steep headwater streams, the channel bed morphology typically changes from pool-riffle to step-pool to cascade morphologies [*Montgomery and Buffington*, 1997], the grain size distributions coarsens [e.g., *Knighton*, 1980; *Rice and Church*, 1998], and immobile boulders and bedrock constrictions become more abundant [e.g., *Nitsche et al*., 2011; *Wohl*, 2000; *Yager et al*., 2007]. These 'form' or 'macro' roughness elements increase flow resistance in steep streams and reduce the flow energy available to entrain and transport sediment [*Nitsche et al*., 2011; *Rickenmann and Recking*, 2011]. To account for flow resistance due to macro-roughness, several flow resistance partitioning approaches have been developed, going as far back as the method of *Meyer-Peter and Müller* [1948]. In these approaches, energy losses are typically described by empirical equations based on roughness measures such as the characteristic grain sizes D_{65} [*Wilcock et al*., 2009] or D_{84} [*Chiari and Rickenmann*, 2011; *Chiari et al*., 2010; *Rickenmann and Recking*, 2011], step height and spacing [*Egashira and Ashida*, 1991], sequences of gravel bars and pool-riffles

[*Millar*, 1999; *Millar and Quick*, 1994], boulder concentrations [*Pagliara and Chiavaccini*, 2006; *Whittaker et al*., 1988] or boulder protrusion [*Yager et al*., 2007].

A second effect reducing the flow energy available for bed load transport at steep slopes is the increased threshold of particle entrainment, often quantified as a critical shear stress (τ_c) [*Shields*, 1936]. The increased τ_c observed at steep slopes [*Bunte et al*., 2013; *Camenen*, 2012; *Ferguson*, 2012; *Lamb et al*., 2008; *Prancevic and Lamb*, 2015; *Recking*, 2009; *Shvidchenko et al*., 2001] might be explained by an increased bed stability due to interlocking of bed particles [*Church et al*., 1998], increased friction angles, grain emergence above the flow, increased turbulence, or reductions in water density due to aeration [*Lamb et al*., 2008]. Alternatively, the increase of τ_c with increasing bed gradients may be mainly the result of estimating τ_c from the total boundary shear stress, without explicitly accounting for increased flow resistance [*Schneider et al*., 2015b]. Accordingly, in a recent field study, increasing critical shear stresses with increasing slope were explained by increased energy losses due to form roughness [*Prancevic and Lamb*, 2015].

Sediment transport predictions in steep channels are further complicated by the fact that sediment supply is spatially and temporally more variable (and often more limited) in steep channels compared to lower-gradient channels, due to a greater abundance of relatively stable bed patches [*Nelson et al*., 2009; *Yager et al*., 2012b], topographic controls such as bar morphology [*Laronne and Duncan*, 1992; *Lisle and Hilton*, 1999], accumulations of immobile boulders [*Garcia*, 1999; *Laronne et al*., 2001], and the development of a coarse immobile surface layer, which protects a finer subsurface layer from the flow (bed armoring) [*Bathurst*, 2007]. Furthermore, the sediment availability often depends on the flow stage: with increasing flow stage the fine sediments are first flushed out, then the gravel bed surface layer breaks up, and finally the entire step-pool topography is destroyed, increasing the sediment supply dramatically. These effects are often described with two- or three-phase transport models [*Bathurst et al*., 1987; *Beschta*, 1987; *Ryan et al*., 2005; *Warburton*, 1992] . Sediment is often less available for transport in steeper streams because their alluvial cover is usually thinner, their percentage of bedrock is often greater and their sediment supply from upstream is often smaller [*Buffington and Montgomery*, 1997].

If the factors described above (which are typical for steep streams) are not considered in bed load transport equations (which were typically developed for low-gradient rivers), bed load transport will often be overestimated by orders of magnitude [*Bathurst et al*., 1987; *Chiari and Rickenmann*, 2011; *Lenzi et al*., 1999; *Nitsche et al*., 2011; *Rickenmann and Recking*, 2011; *Rickenmann et al*., 2012; *Schneider et al*., 2015b; *Yager et al*., 2007, 2012a]. Thus, to accurately predict bed load transport rates at steep slopes, one has to consider the increased flow resistance and critical conditions for initiation of motion as additional controls on bed load transport. *Schneider et al*. [2015b] used an extensive field data set covering bed gradients from 0.0005 to 0.11 m m^{-1} to show that systematic bed load transport overestimation at steep slopes can be avoided through a simple flow resistance partitioning approach that uses a reduced energy slope based on D_{84} [*Chiari and Rickenmann*, 2011; *Chiari et al*., 2010; *Rickenmann and Recking*, 2011]. However, to our knowledge, bed load transport predictions for very steep channel conditions (gradients larger than about 0.2), and consequently for extremely rough hydraulic conditions, have not been extensively tested yet; for such channel gradients a transition to transport conditions typical of debris floods and debris flows may be expected [*Prancevic et al*., 2014; *Rickenmann*, 2012].

In this study, we present a bed load transport field data set from a very steep mountain stream that provides a natural experiment for exploring how bed load transport varies with stream gradient [*Schneider et al*., 2015a]. Whereas the bed gradient increases by roughly one order of magnitude from 0.028 to 0.38 m m^{-1} over the 1 km studied stream section, flow discharge and width remain approximately constant during glacier and snowmelt runoff in summer. The bed load transport data are complemented by an extensive data set on channel bed topography and hydraulic conditions [*Schneider et al*., 2015a]. We investigated how bed load transport rates and annual bed load budgets change with increasing bed gradients. We further tested whether flow resistance [*Rickenmann and Recking*, 2011; *Schneider et al*., 2015a] and bed load transport equations [*Schneider et al*., 2015b; *Wilcock and Crowe*, 2003] validated at lower-gradient channels are able to reproduce the observed bed load behavior at much steeper slopes.

Figure 1. (a) Bed load transport study reach on the low-gradient glacier forefield with $S=0.028$ m m^{-1} and a bankfull width of about 6.8 m. The inset shows researchers emptying the bed load traps. (b) Steep study reach with $S=0.38$ m m^{-1} and a bankfull width of about 5.9 m. (c) Water intake downstream of the steep study reach, showing the Swiss plate geophone array and the Tyrolean weir that separates the coarse bed load from the water. (d) Coarse bed load Q_b with $D>30$ mm is transported over the Tyrolean weir to the depositional area (covered here by white tarp from which the sediment was collected for weighing during geophone calibration periods). Fine sediments with $D\leq 30$ mm fall through (rather than pass over) the Tyrolean weir and are removed from the water in a settling basin built inside the concrete structure on the river left side of the weir.

2. Field Site and Methods

2.1. Riedbach Field Site

The Riedbach is a glacier-fed mountain stream located in the Matter Valley, Ct. Valais (Switzerland). Below the glacier snout (~2180 m a.s.l.), the Riedbach flows through a reach on the glacier forefield characterized by bed gradients ranging from about 2.8% to 6% (Figures 1a and 2a). The Riedbach then transitions to a very steep reach with bed gradients ranging from 30% to 40% (Figures 1b and 2b) as it plunges into the Matter valley. At the downstream end of this steep reach, the Kraftwerke Mattmark AG (KWM) operates a water intake for hydropower generation (Figure 1c). At the water intake (1800 m a.s.l.), the Riedbach drains a watershed of 15.8 km^2, 53% of which is covered by the glacier (as of 2001; Vector25 © 2014 swisstopo (DV033594)). The catchment elevation range is 1800–4300 m a.s.l.

2.1.1. Streambed Characteristics and Sediment Supply

In the Riedbach study reach, bed sediment coarsens and bed roughness increases with increasing bed gradient. The characteristic grain sizes $D_{30}/D_{50}/D_{84}$ increase by factors of five or six, from 0.03/0.06/0.17 to 0.16/0.38/0.91 m (Table 1). These characteristic grain sizes are derived from averaged grain size distributions (GSDs). On the glacier forefield two GSDs were determined, one on the low-flow channel and one on the high-flow channel. A variant of the *Wolman* [1954] procedure was used, in which a sampling frame indicates particles to be included in the sample, and particle sizes were measured with a template based on >400 samples [*Bunte et al*., 2009, 2013]. On the steep reach, grain size distributions were determined by line-by-number samplings [*Fehr*, 1987] at three cross sections, yielding ~950 samples in total. Averaged grain size distributions were derived from combining the individual measurements from all of the sampling locations. In Table 1 the "min" and "max" grain sizes for the flat reach refer to the grain size distributions of the high-flow and low-flow channels respectively.

The characteristic grain size D_{84} was used as a proxy for streambed roughness. Roughness heights were also measured more directly from bed surface topography, using standard deviations and semivariances

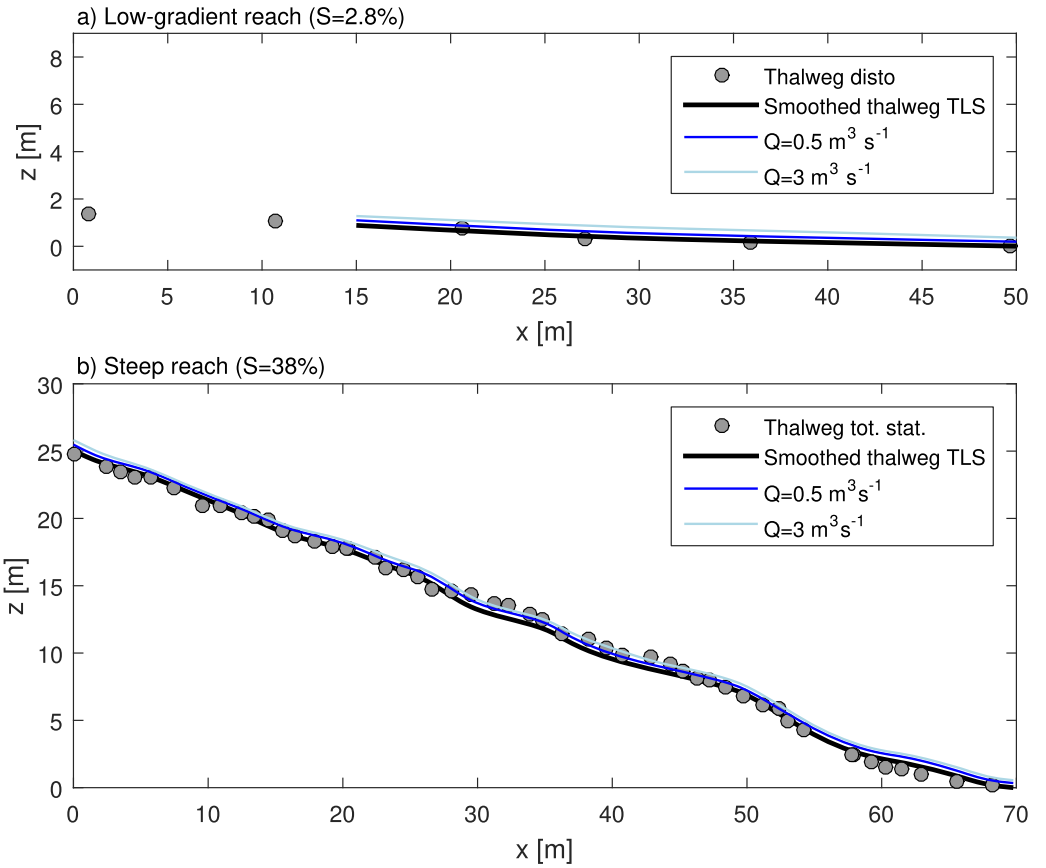

Figure 2. Longitudinal profiles for (a) the low-gradient (glacier forefield) reach and (b) the steep reach, based on terrestrial laser scans (black line) and surveying with total stations or laser distance meters (gray filled circles). The figures have no vertical exaggeration. Colored lines show estimated water surface elevations at 0.5 and 3 m^3s^{-1}, respectively.

derived from terrestrial laser scanning during autumn low-flow conditions. However, these roughness measures and the characteristic grain sizes showed similar functional relationships with channel slope, and were equally effective in explaining the observed hydraulic conditions via flow resistance equations [*Schneider*

Table 1. Streambed Characteristics in the Low-Gradient and Steep Reaches

			Low-Gradient Reach[a]			Steep Reach[b]
Slope S (m m^{-1})			0.028			0.38
Reach length (m)			52			111
Bankfull flow (m^3/s)[c]			3.0			4.0
Bankfull[d] width (m)/depth (m)/velocity (m/s)			6.8/0.34/0.51			5.9/0.39/0.53
	Avg.	Min	Max	Avg.	Min	Max
D_{30} (m)	0.03	0.02	0.03	0.16	0.14	0.19
D_{50} (m)	0.06	0.05	0.07	0.38	0.36	0.45
D_{84} (m)	0.17	0.16	0.18	0.91	0.75	1.28
D_{90} (m)	0.21	0.2	0.22	1.16	0.83	1.49
D_{sg} (m)[e]	0.05	0.04	0.05	0.21	0.18	0.27

[a]The characteristic grain sizes are based on the average GSD of two pebble counts. The finer grain size distribution (with min. characteristic grain sizes) was determined over the full width of the channel that is wetted at high flows; the coarser grain size distribution (with max. characteristic grain sizes) was determined over the narrower, deeper part of the channel that is wetted at both high and low flows.

[b]The characteristic grain sizes are derived from averages of line-by-number GSDs determined over three cross sections in the steep reach (no distinction between low- and high-flow channels). Min and max values refer to the finest and the coarsest of the three distributions.

[c]Low-gradient bankfull flow was derived from *Bunte et al.* [2013], steep bankfull flow was approximated with the effective discharge from the magnitude frequency analysis of sediment transport rates [*Schneider et al.*, 2015a].

[d]Bankfull hydraulic parameters are based on the hydraulic geometry relations given in *Schneider et al.* [2015a]

[e]D_{sg} = geometric mean of stream bed surface.

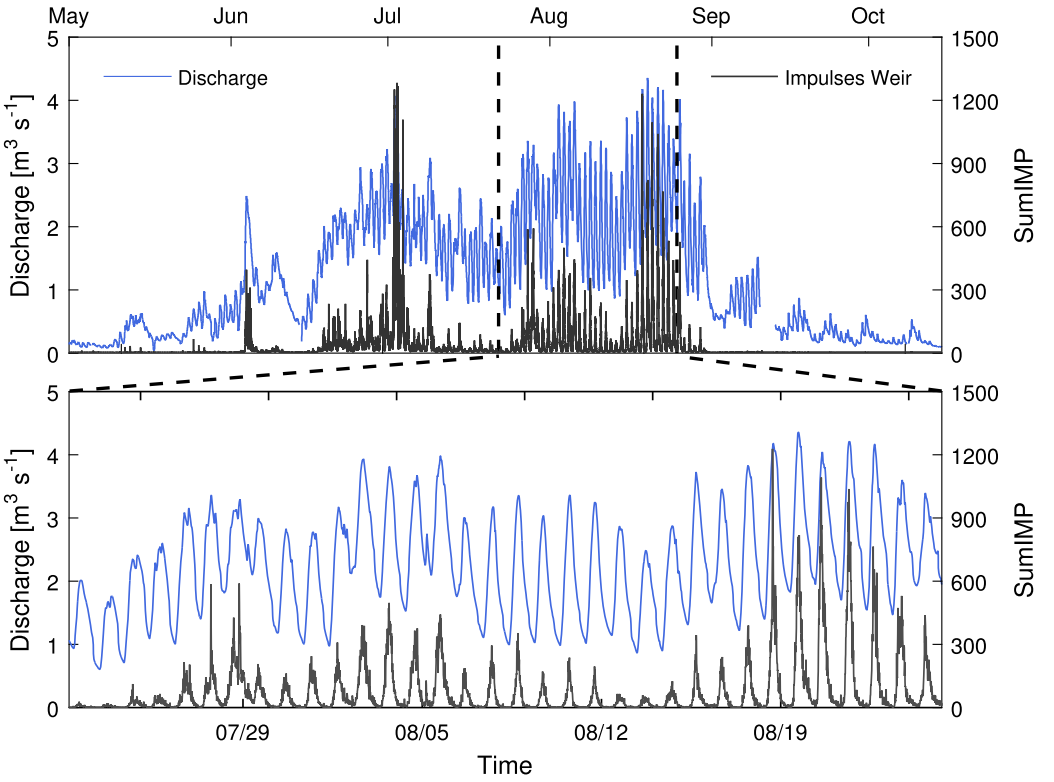

Figure 3. (top) Discharge and bed load transport (represented here by the number of geophone impulses *SumIMP* measured at the water intake) time series from May to October 2012 and (bottom) an expanded view from 29 July 2012 to 25 August 2012. The hydrograph (and the bed load transport intensities) are strongly affected by the glacier melt, resulting in daily peak discharges in the late afternoon and annual peak flows in July and August during sunny and warm periods.

et al., 2015a]. Using D_{84} as a proxy for roughness is also justified because in both reaches there are no other large-scale roughness elements such as pronounced step-pool sequences, woody debris or bedrock constrictions.

The main sediment sources are the recent glacier retreat area located about 600 m upstream of the flat study reach [cf. *Schneider et al*., 2015a] (supporting information Figure S1) and the channel bed itself. Sediment supply from the banks can be assumed to play a minor role. On the glacier forefield, the study reach was de-glaciated about 50 years ago [*VAW/ETHZ and EKK/SCNAT*, 2015], the banks are shallow and a dense vegetation cover consisting of grasses and shrubs has developed. In the steep reach, the banks on river left are mainly characterized by exposed bedrock and the banks on river right are characterized by boulders with dense shrub and alpine forest vegetation [*Schneider et al*., 2015a].

2.1.2. Flow Characteristics

The Riedbach is dominated by a glacial runoff regime with pronounced seasonal and diurnal variations in flow discharge rates Q (Figure 3). The maximum flow that can be captured by the water intake is about 4 m^3s^{-1}, which corresponds roughly to the maximum flows due to glacial melt during warm summer periods. However, some flow starts to overpass the water intake at about 1.5–2 m^3s^{-1}. In addition, a small amount of the stream flow is not captured and bypasses the water intake as residual water at all flow levels. An unmeasured small amount of the flow is diverted for irrigation upstream of the water intake. The unmeasured components of the stream flow were assessed to be roughly 20% of the measured flow [*Schneider et al*., 2015a] and the measured flow was thus increased by a factor of 1.2. High flows due to extreme rainfall-driven events cannot be considered in this analysis because flows above 4 m^3s^{-1} are not measured. However, these events occur rarely in the Riedbach catchment and are assumed to play a minor role in the annual sediment and water flow budgets in the present study [cf. *Schneider et al*., 2015a, Figure 9].

Flow discharge rates are assumed to be constant from the glacier forefield to the steep reach because the major part of the flow in all sections is driven by the glacial melt and contributions from rainfall play a minor

role. Furthermore, the catchment area increases only by a factor of 1.1 over the studied stream section, and water inflows from tributaries or groundwater, as well as water removal (e.g., for irrigation purposes), can be neglected. This assumption is supported by discharge estimates from dye tracer experiments conducted along the entire 1 km study reach [*Schneider et al*., 2015a].

Flow discharge rates are measured inside the settling basin at the water intake at 10 min intervals. For the study period 2009–2015, discharge records are about 95% complete, with about 5% gaps. No difference in data completeness was observed between the summer and the winter seasons, defined here as beginning on April 16 and October 16, respectively. About 1% of the available flows were judged to be implausibly high (considerably above 5 m^3s^{-1}) or low during settling basin flushings. To remove individual erroneous data points, a robust loess smoothing filter was applied (supporting information Figures S1–S8). It was visually confirmed that the daily (plausible) peak flows were not smoothed out and the smoothing span was adjusted manually where necessary. Some periods showed negative discharge, which can be explained by the poor definition of the flow stage-discharge relation at low flows. These occurred predominantly during the winter, making up 11% of the winter study period compared to only 3% during summer.

2.2. Bed Load Transport Measurement

2.2.1. Low-Gradient Reach: *Bunte* Bed Load Traps

In the low-gradient study reach, bed load transport rates were determined using portable bed load traps [*Bunte et al*., 2004, 2009]. The bed load traps consisted of an aluminum frame (0.3 x 0.2 m opening) with a large nylon net attached at its downstream side to capture bed load (Figure 1c). The large net facilitates long sampling times (typically an hour) and large sample volumes (up to 20 L), thus improving the chances of proportionally sampling the coarse bed load fractions that move less frequently. The traps were placed onto ground plates that were anchored in the streambed by metal stakes and then strapped to the stakes. The bed load traps were installed in a 1 m sequence (i.e., with 0.7 m spacing between each pair of neighboring frames) over the entire cross section after a 50m-long straight and morphologically homogeneous reach (at Fl#02 as presented by *Schneider et al*. [2015a], Figure 3). The samples were sieved using 2 mm, 4 mm, 10 mm, 20 mm, 32 mm and 64 mm sieves to determine fractional transport rates (supporting information Data Set S1). Fractional transport rates were then converted to the phi-scale (2, 4, 8,. . ., 128 mm) that is used later in this study.

The nylon net had a mesh width of 6 mm, but we observed that considerable amounts of sediment finer than 6 mm were also captured in the trap. The grain size distributions of the bed and the bed load were consistent with a smooth hiding function, down to and including the 4–10 mm grain size class. However, the 2–4 mm size class was strongly under-represented in the sampled load relative to the same hiding function, consistent with under-catch of these finer grains. The corrected annual bed load volumes based on a bed load transport rating curve that accounts for the underestimated finest 2–4 mm grain size class would be roughly 50% higher. This uncertainty is smaller than the general uncertainty related to the choice of the rating curve (1-piece or 2-piece), we therefore consider the $\geq$4 mm grain size classes only within this study.

2.2.2. Steep Reach: Swiss Plate Geophone System

Bed load transport at the downstream end of the steep study reach has been monitored since 2009 using the Swiss plate geophone system [*Rickenmann et al*., 2014]. The geophone system is an indirect sediment transport measurement method that has been applied primarily in the field [e.g., *Rickenmann et al*., 2014; *Schneider et al*., 2014; *Turowski and Rickenmann*, 2011; *Turowski et al*., 2011; *Wyss et al*., 2016a], and recently a flume-based procedure for the signal interpretation was tested against some of the field calibration measurements [*Wyss et al*., 2016b, 2016c]. Seven plates, each 0.5 m wide and 0.36 m long (in the stream-wise direction) were installed in an array over the entire 3.5m-wide artificial approach flow channel in front of the water intake (Figure 1c). Vibrations produced by impacting particles are registered by geophone sensors. Each time the signal exceeds a predefined threshold of 0.1 V, an impulse count is recorded [*Rickenmann et al*., 2014]. The sum of impulses is stored for each minute when transport occurs. Only grains with diameters larger than about 20 mm produce vibrations that result in impulse counts that can be clearly distinguished from background noise. The number of registered geophone impulses is stored together with the discharge data at 10 min intervals for each plate. For all analyses presented here, impulses of all individual plates were summed over the entire cross section (here abbreviated *SumIMP*, supporting information Data Set S1). Downstream of the geophone array, a grate with a spacing of 30 mm covers the water inlet, causing sediments with D>30 mm to be transported over the intake and water and sediment with

$D<30$ mm to be captured by the intake (this structure is termed a Tyrolean weir; see Figure 1c). The captured water and fine sediments are separated from each other in a 18 m long settling basin, which is flushed whenever a certain sediment level is reached (Figure 1d).

To quantify absolute transport rates, geophone impulses were compared to short- and long-term observations of the volume of the transported sediment. To measure the coarse material deposits ($D>30$ mm, corresponding to the Tyrolean weir grid spacing), a retention fence was installed downstream of the water intake in 2010 and 2011 (Figure 1d). Short-term records were derived by covering the ground with tarps and collecting the transported sediment for weighing and sieving the following day. Volumes of sediment deposited over longer periods were surveyed using a terrestrial laser scanner at 1–2 week intervals (ScanStation C10, Leica Geosystems). The deposited sediment volumes were converted to mass, assuming a bulk density of 1700 kg m^{-3} including pore volume. Some finer sediments ($D<30$ mm) were deposited and observed downstream of the water intake despite the 30 mm grid spacing, comprising about 20% (by volume) of the sediments deposited downstream of the intake. However, for convenience, in this study these finer sediments were assigned to the "coarse" bed load volumes, whereas the sediments that passed the Tyrolean weir in the settling basin are labeled as "fine" sediments. Doing so is justified because the "coarse" bed load transport is not the main focus of the paper, but instead the "total" bed load transport which is calculated as the "coarse" bed load plus the "fine" sediments from the settling basin.

Volumes of transported fine sediment that passed through the Tyrolean weir and were deposited in the settling basin (Figure 1d) were estimated from the number of basin flushings during the long-term measurement periods (8.2 m^3 of sediment per flushing). For the short-term periods, the volume of fine sediment was estimated by manual and continuous surveys of the depositional surface in the settling basin, using a sonar and two fill-level sensors that automatically trigger the basin flushing procedure. However, for short-term measurements at very low flows, no significant changes in the recorded sediment volumes could be observed; in these cases, a factor of 2.4, corresponding to the long-term average of the ratio between fine and coarse sediment, was used to estimate the volume of fine sediment.

2.3. Bed Load Transport Prediction

2.3.1. Hydraulic Parameters

Bed load transport rates are typically described as a function of the hydraulic forcing, which can be expressed by, e.g., flow discharge, stream power or shear stress. In this study, bed load transport is described either as a function of shear stress τ (equation (1a)) or dimensionless shear stress τ^* (equation (1b)), both of which are proportional to the hydraulic radius r_h (m) and stream bed gradient S (m m^{-1})

$$\tau = \rho g r_h S \tag{1a}$$

$$\tau_i^* = \frac{\tau}{(\rho_s - \rho) g D_i} \tag{1b}$$

where g is gravitational acceleration (m s^{-2}), ρ is water density (kg m^{-3}), ρ_s is sediment density (kg m^{-3}) and D is the diameter of a particle or grain size fraction (m).

Hydraulic parameters such as flow depth, hydraulic radius and flow velocity were back-calculated from measured flow discharge at the water intake using the continuity equation, the variable power equation (VPE) of *Ferguson* [2007] (equation (2)), and measured cross sections at 0.2 m intervals along the thalweg, derived from a high-resolution laser scan DTM (see supporting information Data Set S2) [*Schneider et al*., 2015a]:

$$u/u* = \sqrt{\frac{8}{f_{tot}}} = \frac{a_1 a_2 (r_h/D_{84Surf})}{\sqrt{a_1^2 + a_2^2 (r_h/D_{84Surf})^{5/3}}} \tag{2}$$

In equation (2), u is flow velocity (m s^{-1}), u^* is shear velocity $u^* = (g r_h S)^{0.5}$ and r_h/D_{84} is the relative flow depth. The friction factor f_{tot} refers to the total flow resistance. The VPE parameter $a_2 = 3.97$ was fitted to measured flow velocity and bed roughness parameters presented by *Schneider et al*. [2015a]. Flow conditions at large relative flow depths are primarily controlled by the parameter a_1 in the VPE. However, in the Riedbach we had no velocity observations with relative flow depths considerably larger than about 1 (supporting information Figure S9) from which we could estimate a_1. We therefore used the value $a_1 = 6.5$ as suggested by *Ferguson* [2007] and *Rickenmann and Recking* [2011], in both equations (2) and (4) (see section

2.3.2). The hydraulic parameters were calculated for each cross section separately and then averaged for each study reach, because it was not possible to derive a representative mean cross section due to the irregular bed topography.

2.3.2. Flow Resistance Partitioning

To account for energy losses due to form roughness, a flow resistance partitioning approach was used [*Chiari and Rickenmann*, 2011; *Chiari et al*., 2010; *Nitsche et al*., 2011; *Rickenmann*, 2012; *Rickenmann and Recking*, 2011; *Schneider et al*., 2015b]. In this approach, the dimensional applied shear stress (equation (1)) is computed using a reduced energy slope S_{red} (equation (3)) instead of the real channel slope:

$$S_{red}=S\left(\sqrt{\frac{f_0}{f_{tot}}}\right)^{e} \tag{3}$$

Equation (3) is based on a flow-resistance partitioning between a base level flow resistance (f_0) and the total resistance (f_{tot}), which includes additional resistance due to macro-roughness elements at relatively small flows. The exponent $e=1.5$ was established in previous studies [*Meyer-Peter and Müller*, 1948; *Nitsche et al*., 2011]. Total resistance (f_{tot}) is determined with equation (2). The base level resistance (f_0) is calculated by extrapolating the Manning-Strickler relation to small relative flow depths, using the resistance coefficient $a_1=6.5$ [*Ferguson*, 2007; *Rickenmann and Recking*, 2011] (equation (4)).

$$\sqrt{\frac{8}{f_0}}=a_1\left(\frac{r_h}{D_{84}}\right)^{0.167} \tag{4}$$

2.3.3. Bed Load Transport Equations

The bed load transport equations are based on the fractional transport model of *Wilcock and Crowe* [2003] (abbreviated WC), which describes the dimensionless bed load transport rate W^*_i (equation (5)) as a function of the ratio of the applied shear stress τ_i to the reference shear stress τ_{ri} ($\theta=\tau_i/\tau_{ri}$) per grain size fraction D_i (equation (6)).

$$W_i^*=\frac{Rgq_{biVol}}{F_i u^{*3}} \tag{5}$$

In equation (5) F_i is the proportion of the grain size class i derived from the bed surface grain size distribution, q_{biVol} is the volumetric fractional bed load transport rate (excluding porosity) per unit width $m^3s^{-1}m^{-1}$, $u^*=(\tau/\rho)^{0.5}$ is the shear velocity, and $R=(\rho_s/\rho)-1$.

$$W_i^*=\begin{cases}0.002\theta^{7.5} & \text{for } \theta < 1.35\\ 14\left(1-\frac{0.894}{\theta^{0.5}}\right)^{4.5} & \text{for } \theta \geq 1.35\end{cases} \tag{6}$$

The reference shear stress τ_{ri} of each grain size fraction D_i is determined as a function of the mean grain size D_m (as approximated here with the D_{50} of the streambed surface distribution, see also *Schneider et al*. [2015b]) and the reference shear stress τ_{rDm} using a dimensional form of a hiding function (equations (7) and (8)):

$$\tau_{ri}=\tau_{rDm}\left(\frac{D_i}{D_m}\right)^{b} \tag{7}$$

$$b=\frac{0.67}{1+\exp\left(1.5-\frac{D_i}{D_{50}}\right)} \tag{8}$$

Instead of using the sand to estimate the reference shear stress τ_{rDm}, as originally suggested by *Wilcock and Crowe* [2003], here an average dimensional reference shear stress, back-calculated from a dimensionless reference shear stress of $\tau^*_{rDm}=0.03$, was used. The value $\tau^*_{rDm}=0.03$ generally described the reference conditions well for a large field data set with a wide range of bed gradients [*Schneider et al*., 2015b], when additional resistance due to macro-roughness at steep slopes was considered by using equation (3).

In addition to equation (6), we also used the slightly modified field-based equations presented by *Schneider et al*. [2015b] to predict bed load transport. These modified versions were derived from a large field data set of bed load transport observations covering a wide range of bed gradients. The first equation (equation (9),

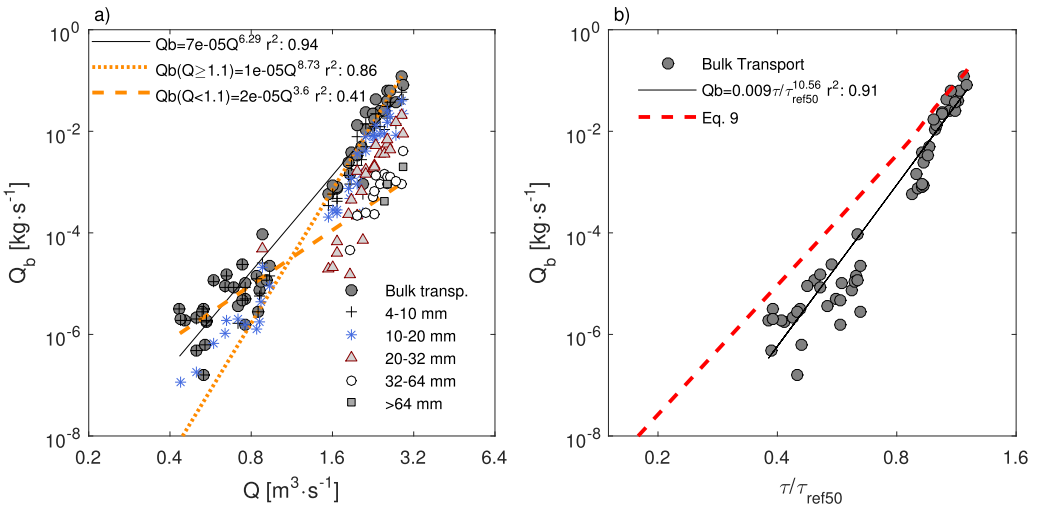

Figure 4. (a) Low-gradient reach bulk and fractional bed load transport rates as functions of discharge and (b) the ratio of shear stress to reference shear stress τ/τ_{ref50}. Transport rates were derived from the bed load trap measurements and refer to grain sizes $D \geq 4$ mm. The red-dashed line (Figure 4b) was derived from the dimensionless transport equation (equation (9)) and equation (5).

abbreviated SEA-1) is based on a dimensionless reference shear stress that remains constant as bed gradient changes ($\tau^*_{rDm}=0.03$); it is applied with a reduced bed shear stress according to equation (3).

$$W_i^* = \begin{cases} 0.002\theta^{6.82} & for\ \theta < 1.33 \\ 14\left(1-\frac{0.894}{\theta^{0.5}}\right)^{4.5} & for\ \theta \geq 1.33 \end{cases} \quad (9)$$

The second equation (equation (10), abbreviated SEA-2) accounts for increasing total resistance with increasing channel gradient (as a modeling approach) via an empirical equation expressing the increasing dimensionless reference shear stress with increasing channel gradient (equation (11)). To calculate bed load transport, equations (10) and (11) are then combined with the total boundary shear stress (without reducing the energy slope as in equation (3)), as demonstrated by *Schneider et al.* [2015b]. Furthermore, equation (6) was tested without any correction for additional (macro) roughness, neither for the applied shear stress nor for the reference shear stress τ_{ri} in $\theta = \tau_i/\tau_{ri}$ (abbreviated WC'). Finally, further approaches that positively relate the reference shear stress with bed slope [*Bunte et al.*, 2013; *Lamb et al.*, 2008; *Mueller et al.*, 2005] (similar to equation (11)) were tested with equation (10). However, because these approaches did not yield substantially better performance, their results are shown in the supporting information only.

$$W_i^* = \begin{cases} 0.002\theta^{13.7} & for\ \theta < 1.2 \\ 14\left(1-\frac{0.85}{\theta^{0.7}}\right)^{4.5} & for\ \theta \geq 1.2 \end{cases} \quad (10)$$

$$\tau^*_{rDm} = 0.48S^{0.45} \quad (11)$$

3. Results

3.1. Measured Bed Load Transport

3.1.1. Low-Gradient Reach (*Bunte* Bed Load Trap System)

Measured bulk bed load transport rates $Q_b \geq 4$ mm for the low-gradient reach on the glacier forefield ranged from about 10^{-7} to 10^{-1} kg s^{-1} (corresponding to a few grains of fine gravel to about 350 kg bed load mass per hour) for the observed discharge rates ranging from about 0.5 to 3 m^3 s^{-1}. It was not possible to operate the traps during higher discharges than presented here. The bed load rating curves can be described by a power law with an exponent of about 6.3 (Figure 4a) (equation (12))

$$Q_b = (70.7 \pm 9.5) \times 10^{-6} Q^{(6.3 \pm 0.22)} \quad r^2 = 0.94 \quad (12)$$

where the uncertainties are standard errors. The units are kg s^{-1} for Q_b and m^3 s^{-1} for Q in both equations (12) and (13). However, from the data one might also propose two separate rating curves, approximately separated by a critical discharge $Q_c \sim 1.1$ m^3 s^{-1} (Figure 4) (equation (13)).

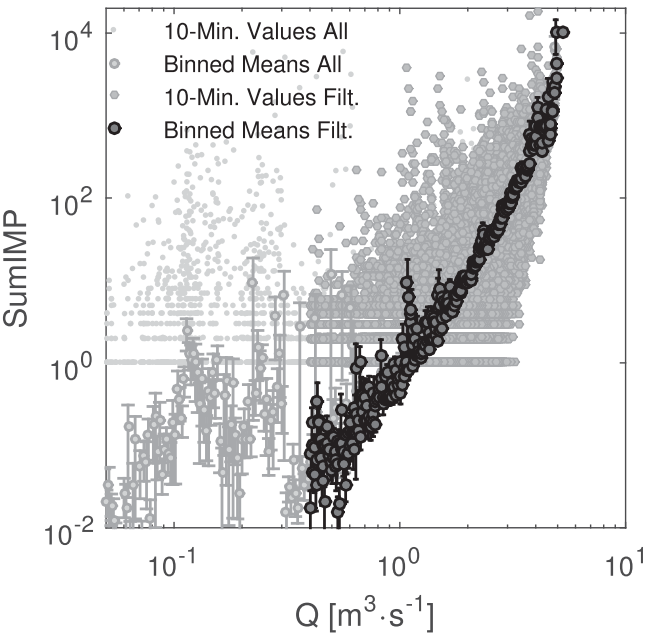

Figure 5. Geophone impulses *SumIMP* (10 min values) as a function of flow discharge in the steep reach. Light gray small dots are considered to be implausible (see text); values shown by medium gray circles are considered to be plausible. Binned means (darker gray circles, shown with error bars based on the standard error) include zero values of *SumIMP*.

$$Q_b = (20.8 \pm 6.7) \times 10^{-6} Q^{(3.59 \pm 0.87)} \quad r^2 = 0.41 \text{ for } Q \leq 1.1 \text{ m}^3\text{s}^{-1} \tag{13a}$$

$$Q_b = (11.6 \pm 5.4) \times 10^{-6} Q^{(8.73 \pm 0.72)} \quad r^2 = 0.86 \text{ for } Q \leq 1.1 \text{ m}^3\text{s}^{-1} \tag{13b}$$

In the following, equations (12) and (13) are termed the 1-piece and 2-piece rating curves, respectively. For discharge rates up to about 1.1 m^3s^{-1}, measured bed load transport rates are rather scattered (lower r^2 in equation (13a) compared to equation (13b)) and only grains <20 mm are transported (Figure 4). The scattering of fractional bed load transport rates around a mean trend line generally decreases with increasing flow rates, resulting in a well-defined bed load rating curve. At higher flow discharge rates, coarser sediments were transported (Figure 4a).

3.1.2. Steep Reach (Swiss Plate Geophone System)

The counts of geophone impulses (*SumIMP*) as a measure of bed load transport intensity generally follow the annual and daily variations in flow discharge *Q* (Figure 3). The 10 min *SumIMP* values are a highly scattered function of *Q*, especially at lower flows (Figure 5). However, for $Q > 0.4$ m^3s^{-1} the average *SumIMP* exhibits a clear increasing trend with increasing *Q*. For $Q < 0.4$ m^3s^{-1}, on the other hand, no systematic relationship between *SumImp* and *Q* can be identified (Figure 5). The points that combine high *SumImp* values and low *Q* mostly arise during winter, when discharge is too low to support significant bed load transport, suggesting that ice formation or some other technical problem may be responsible. To remove implausible values of *SumIMP* at low discharges, we therefore only consider the summer season (defined here from April 16 to October 15), because it is assumed that the winter season plays a minor role in the annual budgets of water and sediment transport. Doing so removes only 8% of the total runoff (between 2009 and 2015), and 5% of the total impulses. Furthermore, any other impulses for $Q < 0.4$ m^3s^{-1} were removed from the analysis, which reduces the total *SumIMP* by another 1%. Thus, the following analysis considers only the remaining 94% of *SumIMP*, collected during the summer season and for $Q \geq 0.4$ m^3s^{-1} (dark gray circles in Figure 5).

The correlations between the number of registered impulses *SumIMP* and the measured coarse ($D > 0.03$ m) and total bed load weights Q_b (in kg s^{-1}) are well defined, with r^2 values larger than 0.9 for both linear (zero intercept; Figure 6a) and power law regression equations (Figure 6b). The trends derived from bed load volumes determined from long-term volumetric measurements using the laser scanner (triangles in Figure 6b) correspond well to those derived from short-term manually weighted samples (squares in Figure 6b). The trend derived from the short-term measurements is slightly steeper (*total bed load mass* = 0.54*SumIMP*, $r^2 = 0.49$) than the trend from the long-term measurements (*total bed load mass* = 0.53*SumIMP*, $r^2 = 0.9$). In comparable studies (supporting information Figure S10), linear relations were used to calibrate the geophone signals. However, for the Riedbach the linear relation deviates from the measurements at low values (Figure 6b), therefore here we use a power-law equation (equation (14)) that slightly better represents the entire range of bed load measurements (uncertainties refer to standard errors):

$$Q_b = (0.102 \pm 0.046) SumIMP^{(1.207 \pm 0.071)} \quad r^2 = 0.953 \quad (\text{total bed load}) \tag{14a}$$

$$Q_b = (0.032 \pm 0.007) SumIMP^{(1.158 \pm 0.028)} \quad r^2 = 0.992 \quad (\text{coarse bed load}) \tag{14b}$$

The Riedbach relation between coarse material and *SumIMP* closely follows the calibration curves from other mountain streams equipped with geophone sensors, especially the Erlenbach (CH) and the Rofenache

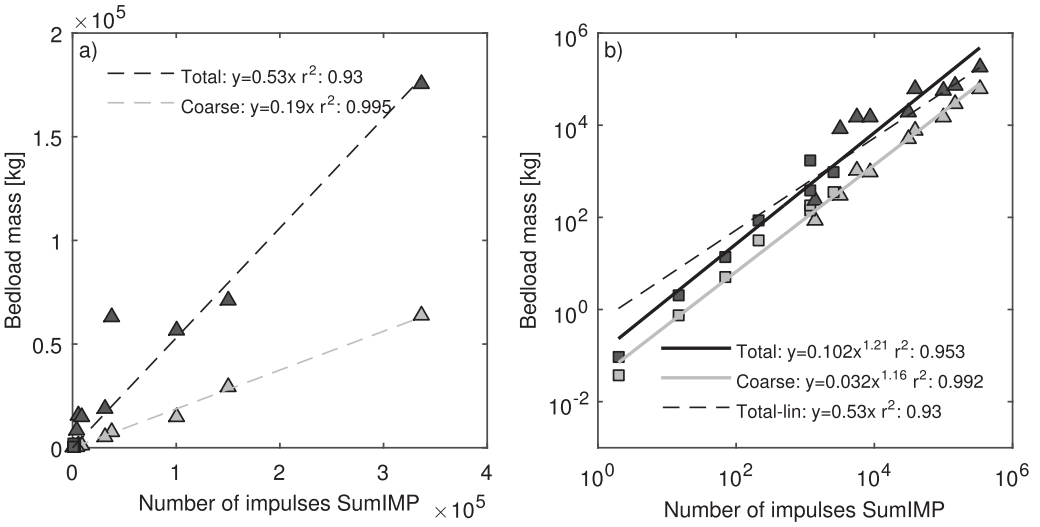

Figure 6. Measured bed load masses related to the number of summed geophone impulses *SumIMP*, on a) linear and b) logarithmic scales, respectively. Gray and black symbols refer to coarse (>30 mm) and total bed load, respectively. Squares show short-term manually collected and weighed bed load measurements. Triangles show long-term volumetric changes of the sediment deposits downstream of the water intake. The intercepts of the linear regression lines are set to zero.

(A) (supporting information Figure S10). The relation for the total bed load plots somewhat to the right of the other relations, possibly because the Riedbach relation includes finer grain sizes compared to the other streams.

The bed load rating curve, based on the binned means of Q_b (determined from equation (14a)), is generally well defined with a $r^2 = 0.95$ equation (15), same units as in equation (12)) (Figure 7a).

$$Q_b = (29.9 \pm 1.4) \times 10^{-5} Q^{(4.6 \pm 0.06)} \quad r^2 = 0.95 \times 10^{-5} \tag{15}$$

Similarly as we did for the low-gradient reach, we also determined a 2-piece rating curve for the steep reach (equation (16)). The two pieces of the rating curve were fitted to two discharge ranges separated by a critical discharge. The overall best performance, determined from the root mean square error (in log-space) for

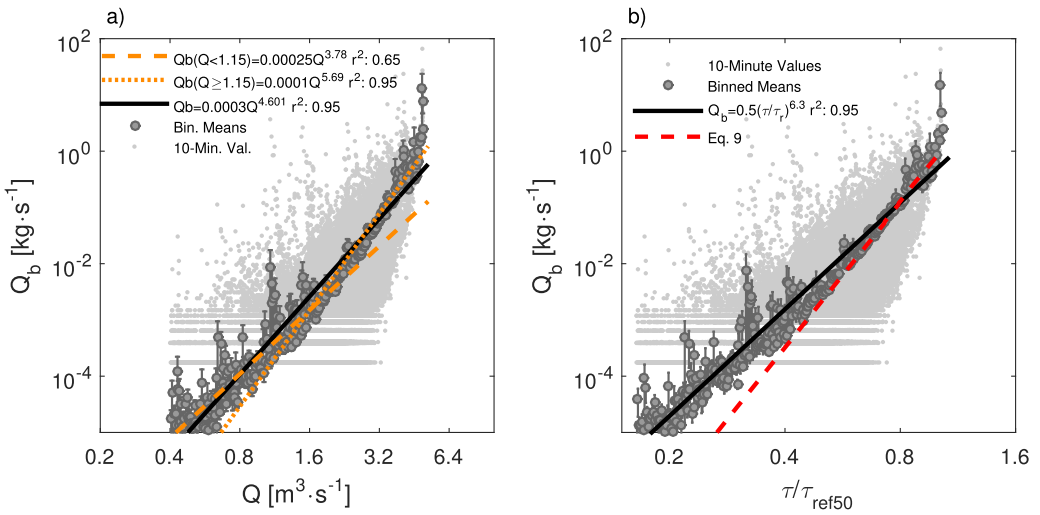

Figure 7. Steep reach bed load transport rates as functions of (a) discharge and (b) the ratio of shear stress to reference shear stress, τ/τ_{ref50}. Dark gray circles show binned means calculated including zero values; error bars show the standard error of each binned mean. The two-piece rating curve (orange lines) was derived by fitting rating curves for a range of critical discharges from 0.8 to 2.5 m^3s^{-1}. The overall best fit was derived for Q_c=1.15 m^3s^{-1}, resulting in an intercept of the lower- and the upper rating curve at ~1.6 m^3s^{-1}. The red dashed line in (b) is derived from the dimensionless transport equation (equation (9)) and equation (5).

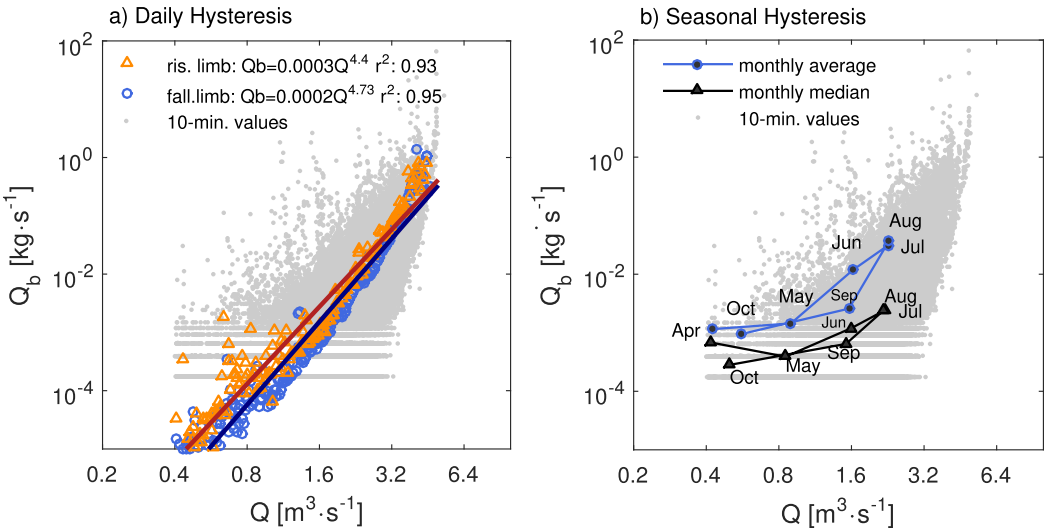

Figure 8. Daily and seasonal hysteresis of bed load transport rates in the steep reach. (a) Orange triangles show the binned means of the daily rising limbs of the hydrograph. Blue circles show the binned means of the daily falling limbs of the hydrograph. Red and blue lines are power-law fits to the rising and falling binned means, respectively. (b) Monthly means (blue circles) and medians (black triangles) of discharge and bed load transport rates. Each data point refers to 1 month starting from April and ending in October. Means do not include zero measurements here.

the resulting 2-piece rating curve, was obtained for a critical discharge of Q_c=1.15 $m^3\ s^{-1}$ (equation (16), same units as in equation (12)). The resulting intercept between the two equations is roughly at 1.6 $m^3\ s^{-1}$ (Figure 7a).

$$Q_b=(25.4\pm1.25)\times10^{-5}Q^{(3.78\pm0.06)}\ \ r^2=0.65\ \ for\ \ Q<1.15\times10^{-5} \tag{16a}$$

$$Q_b=(102.9\pm9.1)\times10^{-6}Q^{(5.69\pm0.09)}\ \ r^2=0.95\ \ for\ \ Q\geq1.15\times10^{-6} \tag{16b}$$

Bed load transport rates measured by geophone impulses can be empirically fitted as a power-law function of τ/τ_{ref50}, where τ_{ref50} is a reference stress based on the D_{50} of the bed (Figure 7b). This empirical relationship lies close to equation (9), especially at higher stresses (Figure 7b).

The geophone measurements indicate that bed load transport rates are affected by small daily and seasonal hysteresis effects (Figure 8). Binned means derived from the rising limb of the daily hydrograph are generally larger than binned means derived from the falling limb (Figure 8a). This effect is stronger at lower flows; at higher flows, the binned means of the rising and falling limbs converge to each other. A weak clockwise seasonal hysteresis is suggested by the monthly means and medians of discharge and bed load transport rates (Figure 8b), with transport rates being higher in June compared to September, and also higher in April compared to October, under comparable mean discharge conditions.

3.1.3. Annual Sediment Loads

The bed load trap rating curves (equations (12) and (13)) and the calibrated geophone signal (equation (14a)) were used to estimate annual sediment budgets for the years 2009–2015 (Table 2, given in volumes excluding pore volume). The standard errors of the coefficients and exponents in equations (12)–(14) were used to estimate uncertainties in the annual loads based on Gaussian error propagation. On the low-gradient reach, where bed load transport rates for $D\geq$ 4mm are inferred from discharge, an additional 10% uncertainty in the discharge measurement was assumed. The resulting uncertainties average 16% for the low-gradient reach and 10% for the steep reach. For the low-gradient reach, annual bed load volumes estimated from the 1-piece rating curve (equation (12); ~55 m^3a^{-1}) are about a factor 3.5 smaller than those estimated from the 2-piece rating curve (equation (13); 192 m^3a^{-1}). The annual bed load volume for the steep reach estimated from the continuous geophone signal (~45 m^3a^{-1} 'total bed load') is close to the bed load volume derived from the 1-piece rating curve for the low-gradient reach, but considerably lower than the loads derived from the 2-piece rating curve.

Table 2. Measured and Predicted Annual Sediment Loads[a]

			Low-Gradient Reach[b]					Steep Reach			
			Equation (12) (1-Piece)	Equation (13) (2-Piece)	Equation (9)			Equation (14a) (Total)	Equation (9)		
Year	ΣQ (10^6 m^3)	ΣQ-Q_c (10^6 m^3)	Q_{bmeas} (m^3)	Q_{bmeas} (m^3)	Q_{bpred} (m^3) avg. GSD	Q_{bpred} (m^3) max. GSD	Q_{bpred} (m^3) min. GSD	Q_{bmeas} (m^3)	Q_{bpred} (m^3) avg. GSD	Q_{bpred} (m^3) max. GSD	Q_{bpred} (m^3) min. GSD
2009	17.2	7.4	45 ± 4.7	111 ± 25	130	43	340	23.8 ± 5.0	22.4	2.1	68
2010	14.6	6.0	60 ± 9.0	206 ± 60	117	41	299	97.2 ± 6.6	32.3	3.0	94
2011	13.9	4.3	36 ± 8.6	128 ± 71	81	28	211	40.1 ± 2.0	19.2	1.8	55
2012	17.2	8.7	78 ± 10.7	270 ± 75	159	55	399	73.6 ± 1.4	42.1	3.9	123
2013	12.3	4.3	34 ± 6.3	106 ± 44	78	27	202	9.4 ± 0.4	17.6	1.6	52
2014	11.9	1.2	6.1 ± 1.5	11.7 ± 7.8	28	9	81	1.0 ± 0.1	2.9	0.3	9
2015	17.7	9.9	123 ± 19.9	514 ± 192	198	71	484	71.9 ± 16.4	68.6	6.3	195
Mean	15.0	6.0	55 ± 8.7	192 ± 68	113	39	288	45 ± 4.6	29	2.7	85
SD	2.2	2.8	35 ± 5.4	152 ± 56	52	19	125	34 ± 5.3	20	1.8	56

[a]Bed load predictions Q_{bpred} are based on equation (9) (calculation approach ID2, see Table 3). Runoff volumes are given in million cubic meters. Sediment volumes are derived from sediment masses assuming a density of 2650 kg m^{-3} (i.e., pore volume not included). A value of $Q_c = 1.5$ m^{3}s^{-1} was used to calculate the effective runoff volume ΣQ-Q_c. Errors in Q_{bmeas} are the standard errors derived from Gaussian error propagation of the standard errors in the coefficients and the exponents in the bed load trap rating curve (equations (12) and (13)) and the geophone calibration line (equation (14)). Max., min., and avg. GSD stands for the coarsest, finest and averaged grain size distribution measured in each reach. SD means standard deviation.

[b]Annual bed load volumes in the low-gradient reach include only grains with $D>4$mm. Adding the unmeasured 2–4 mm grain size class, as estimated in section 2.2.1, would increase the annual volumes by about 50%.

3.2. Predicted Bed Load Transport

Measured bed load transport rates were used to evaluate the performance of two bed load transport equations, equation (6) [*Wilcock and Crowe*, 2003, hereinafter WC] and equations (9) and (10) [*Schneider et al*., 2015b, hereinafter SEA], according to the scheme presented in Table 3 (see section 2.3.3 for details). We evaluated their predictive accuracy using the mean deviation $Mean(Q_{bpred}/Q_{bmeas})$ and a mean discrepancy ratio $Mean(Q_{bpred})/Mean(Q_{bmeas})$; in both cases a value of one indicates a perfect agreement on average, values <1 indicate under-predictions, and values >1 indicate over-predictions. Whereas $Mean(Q_{bpred}/Q_{bmeas})$ is equally affected by the performance of the transport equation over the entire range of bed load transport rates, $Mean(Q_{bpred})/Mean(Q_{bmeas})$ is dominated by the performance at high transport rates, which is of interest for the annual bed load estimates. Additionally, we evaluated both predictive equations based on the percentage of predictions that fall within the one or two orders of magnitude of the measured transport rates (SC_{10} and SC_{100}, respectively) [cf. *Recking*, 2010; *Schneider et al*., 2015a]. Note that for the low-gradient reach, bed load transport predictions and measurements include only grains with $D\geq 4$mm.

The accuracy of bed load transport predictions largely depends on whether potential energy losses due to macro-roughness are taken into account or are neglected. Neglecting these energy losses leads to overestimation of transport rates by up to six orders of magnitude (ID4 in Table 3), whereas the predictive accuracy

Table 3. Bed Load Transport Prediction: Input Parameters and Measures for Comparative Assessment[a]

			Comparative Measures for Low-Gradient Reach (Individual Bed Load Trap Meas.)				Comparative Measures for Steep Reach (Binned Means of *SumIMP*)			
ID	Equation	τ^*_r	Mean (Q_{bc}/Q_{bm})	Mean(Q_{bc})/ Mean(Q_{bm})	SC_{10}	SC_{100}	Mean (Q_{bc}/Q_{bm})	Mean(Q_{bc})/ Mean(Q_{bm})	SC_{10}	SC_{100}
1	WC (equation (6))[b]	0.03	16.58	1.99	66.0	94	0.40	0.41	62	93
2	SEA-1 (equation (9))[c]	0.03	20.19	1.91	64.2	94	0.44	0.42	71	98
3	SEA-2 (equation (10))[d]	Eq. 11	1.07	0.089	83.0	100	3.48	1.11	100	100
4	WC′ (equation (6))[e]	0.03	2.12E+05	327	0.0	2	4.73E+06	1.55E+03	0	0

[a]τ^*_r: reference shear stress; Q_{bc} and Q_{bm}: calculated and measured bed load transport rates, respectively. SC_{10} and SC_{100}: the percentage of predicted transport rates that fall within the one order of magnitude and two orders of magnitude of the observations. Predictions are based on the average grain size distribution given in Table 1.

[b]WC: *Wilcock and Crowe* [2003] accounting for macro-roughness by reducing the applied stress. cf. supporting information Figure S11.

[c]SEA-1: *Schneider et al*. [2015b] accounting for macro-roughness by reducing the applied stress. cf. Figure 9.

[d]SEA-2: *Schneider et al*. [2015b] accounting for macro-roughness by increasing the reference shear stress. cf. supporting information Figure S12.

[e]WC′: *Wilcock and Crowe* [2003] without correcting for additional flow resistance due to macro-roughness.

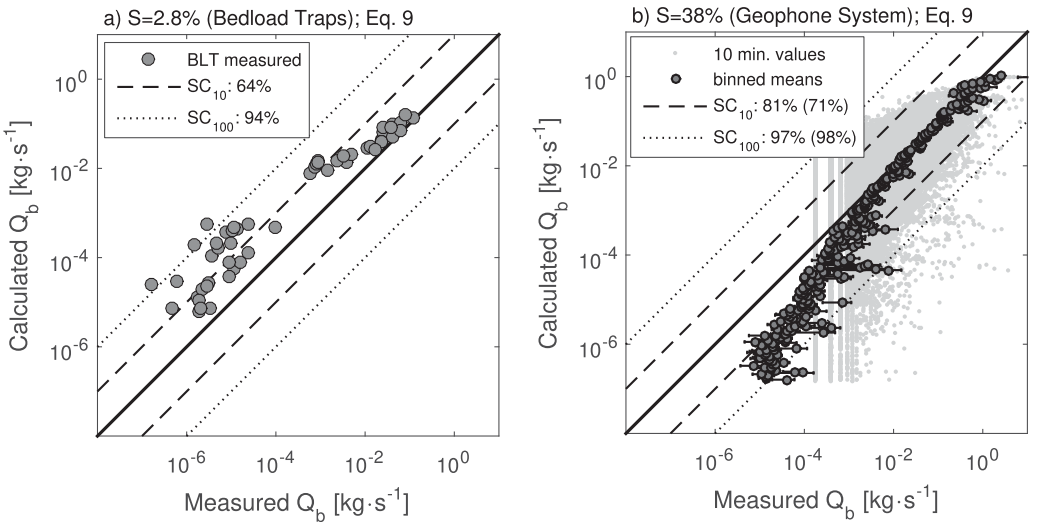

Figure 9. Measured bed load transport rates compared with transport rates predicted from the averaged grain size distribution (Table 1). Calculated hydraulic parameters were based on the fitted VPE [*Schneider et al.*, 2015a] for the (a) low-gradient reach and (b) steep reach. In Figure 9a, the filled circles show bed load trap measurements. In Figure 9b, dark gray circles refer to binned means (in horizontal direction) and the light gray points refer to the 10 min. geophone measurements. The scores SC_{10} and SC_{100} are the percentage of predictions within one order of magnitude (dashed lines) and two orders of magnitude (dotted lines) of the measurements, respectively. In Figure 9b the scores refer to the 10 min. values (the scores in brackets refer to the binned means). On the flat reach, measured and calculated transport rates include only grain sizes $D \geq 4$ mm.

is considerably improved if these losses are taken into account (ID 1-3 in Table 3). The predictions of the *WC* Equation (ID 1) are comparable to those of the *SEA* equation (ID 2 in Table 3) with only minor differences in their measures of performance (Table 3 and Figure 9; supporting information Figure S11). Using the total boundary shear stress as the applied shear stress, in combination with a reference shear stress that varies with bed slope (equation (11)) to account for form roughness (ID3 in Table 3), results in good comparative measures ($Mean(Q_{bpred}/Q_{bmeas})$ and $Mean(Q_{bpred})/Mean(Q_{bmeas})$ close to one) and good reliability scores ($SC_{10}>83\%$ and $SC_{100}=100\%$) for both the low-gradient and the steep reach. However, the transport rates on the low-gradient reach at higher stresses are strongly underestimated, and transport rates on the steep reach are generally overestimated (supporting information Figure S12). Other bed slope-related reference and critical shear stress approaches [*Bunte et al.*, 2013; *Lamb et al.*, 2008; *Mueller et al.*, 2005] were tested with equation (10), but the predictive accuracy of these approaches is not better than using equation (11), and thus the results are presented in the supporting information Table S1.

Bed load predictions based on approach ID2 (Table 3), using equation (9) and the averaged grain size distributions (Table 1), overestimate the individual bed load trap measurements in the low-gradient reach by roughly a factor of twenty at low to medium transport rates (Figure 9a), but perform better at higher rates. This approach predicts annual loads on the low-gradient reach (113 m^3a^{-1} in average, Table 2) that are intermediate between the annual loads derived from the 1-piece and 2-piece rating curves (55 and 192 m^3a^{-1}, respectively). This relatively close agreement shows that the annual sediment budget is largely controlled by the high flows, rather than the low flows where the prediction approach greatly overestimates transport rates. For the steep reach, by contrast, the same approach underestimates transport rates by factors of 5 to 20 or more at low transport intensities, but its predictive accuracy is again much better at higher transport rates. The predicted annual load (29 m^3a^{-1}, Table 2) based on equation (9) for the steep reach is slightly underestimated compared to the measured volume (45 m^3a^{-1}).

These bed load transport predictions are highly sensitive to the grain size distributions that are used. On the low-gradient reach, a grain size distribution with a 31% coarser D_{50} (0.072 instead of 0.055 m) and a 13% coarser D_{84} (0.181 instead of 0.160 m; Table 1) results in predicted annual loads that are smaller by a factor of about ~7.5 (Table 2). In the steep reach, a 25% coarser D_{50} (from 0.36 to 0.45 m) and a 70% coarser D_{84} (from 0.75 to 1.28 m) results in predicted annual loads that are smaller by a factor of about 30 (Table 1 and Table 2). Transport rate predictions based on the finest and coarsest grain size distributions are provided in the supporting information Figures S13 and S14.

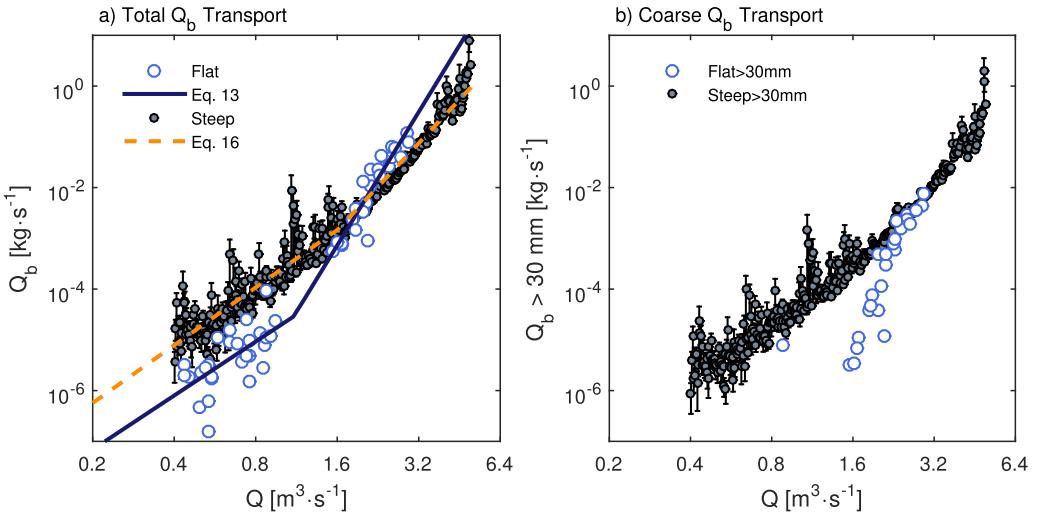

Figure 10. Bed load transport rates as functions of flow discharge for the flat reach (open blue circles) and the steep reach (filled gray circles). The left and right plots show total and coarse (>30 mm) transport rates, respectively. Coarse transport rates on the low-gradient reach were determined from the measured fractional transport rates; coarse transport rates on the steep reach were determined from geophone measurements calibrated using equation (14b) and corrected by the average percentage of fine material found in the downstream deposits (20%, see section 2.2.2).

4. Discussion

4.1. Bed Load Transport (Q_b) Observations

Bed load transport rates and integrated annual loads were determined along a 1 km stream section that spans a roughly 10-fold increase in bed gradient. Measured bed load transport rates show clear positive, but also highly scattered, correlations with flow discharge in both the low-gradient and the steep study reaches (Figures 4 and 7). The scatter in these relationships reflects both measurement uncertainties and the complex nature of bed load transport.

4.1.1. Two-Phase Bed Load Transport

Based on the shapes of the bed load transport - discharge relationships, one might suggest 2-piece rating curves for both reaches, characterized by a break in slope at a critical discharge (Figures 4, 7, and 10). The critical discharge ranges between 1.1 and 1.6 m^3s^{-1} for the two reaches. This observation is in agreement with studies that postulate a distinction between "phase one" and "phase two" transport [*Bathurst et al.*, 1987; *Beschta*, 1987; *Ryan et al.*, 2005; *Warburton*, 1992]. In phase one transport, there is almost no breakup of the coarse, stable surface layer and only fine sediments (sand and fine gravel) are transported (see fractional transport rates in Figure 4a). The transport rates during phase one are strongly related to the mobile sediment supply in pools, behind channel obstructions, or from external sources. This sediment supply is typically highly variable [*Bathurst*, 2007; *Mueller and Pitlick*, 2013; *Recking*, 2012; *Recking et al.*, 2015] and might lead to intermittent bed load transport [*Lajeunesse et al.*, 2010; *Ma et al.*, 2014]. This variable sediment supply at low discharges might explain the increased variability of transport rates for a given discharge observed at low flows in both reaches (Figures 4 and 7). With increasing discharge (phase two transport), the coarse surface (armour) layer breaks up and coarse gravel bed load transport becomes possible (Figure 4a), resulting in increased sediment availability and thus a steeper increase in transport rates with increasing discharge. "Phase three" transport, characterized by break-up of large scale bed forms as observed by *Warburton* [1992] in a steep mountain stream (Rio Cordon, Italy), was not reached at the Riedbach due to the limited discharge range of our observations. The annual loads in the low-gradient reach, as determined from discharge and a rating curve, strongly depend on whether a 1-piece or a 2-piece rating curve is applied. The 2-piece rating curve results in annual loads that are more than a factor of three higher than those obtained from the 1-piece rating curve.

4.1.2. Daily and Seasonal Q_b Variability

Seasonal and daily hysteresis effects result in variable transport conditions for a given discharge and partly explain the scattered bed load transport – discharge relationships in the steep reach (Figure 7). Daily clockwise hysteresis, with higher transport during the rising limb of the hydrograph, was observed in the steep

reach of the Riedbach, primarily at lower discharges (Figure 8a). This hysteresis effect can be explained by the hydraulic conditions: the energy slope (water surface slope) is commonly steeper during rising discharge than during falling discharge [*Bunte et al*., 1996]. Weak clockwise seasonal hysteresis effects can be observed in monthly averages and medians of discharge and bed load transport rates (Figure 8b). The seasonal variability seems to mainly result from individual large events with high transport rates in June, as the hysteresis is clearly weaker in the monthly medians than the monthly means. This may imply the mobilization of sediment sources at higher discharges in June, which could be (partly) depleted by September. While seasonal clockwise hysteresis was documented by *Moog and Whiting* [1998] for some mountain streams in Idaho (USA), seasonal counter-clockwise hysteresis was observed by *Mao et al*. [2014] in a glacial stream in northern Italy, in contrast to the clockwise hysteresis observed in the Riedbach glacial stream.

For the low-gradient reach, no information on daily or seasonal variations in Q_b are available, as measurements were only taken during the daytime and during the summer months. However, if we assume that the low-gradient reach exhibited daily hysteresis similar to that which was observed in the steep reach, the mean annual bed load volumes on the low-gradient reach would be reduced by about 20%, from 55 to 44 m^3a^{-1} (based on the 1-piece rating curve). However, this uncertainty is relatively small compared to the uncertainty that arises from the rating curves themselves (i.e., the factor-of-three difference between the 1-piece and the 2-piece rating curves).

4.1.3. Q_b Comparison and Uncertainties: Flat Versus Steep Reach

Bed load transport rates in the steep reach (hereafter Q_b *steep*) are higher than transport rates on the low-gradient reach (hereafter Q_b *flat*) at lower discharges ($Q < \sim 1.8$ m^3s^{-1}; Figure 10a). However, the different transport rates tend to converge at higher discharges. Q_b *flat* is even somewhat higher than Q_b *steep* at discharge rates larger than about 1.8 m^3s^{-1}. However, considering coarse (>30 mm) bed load transport rates only (Figure 10b), Q_b *flat* and Q_b *steep* are even closer together at higher discharges than the corresponding total transport rates are (Figure 10a).

The differences between Q_b *flat* and Q_b *steep* at high discharges, and the resulting differences in the annual bed load volumes, are difficult to explain. A comparison of Figures 10a and 10b implies that at high flows, fine sediment transport rates are higher on the flat reach than on the steep reach, because total transport rates are higher on the flat reach (Figure 10a) but coarse bed load transport rates are roughly the same on the two reaches at high flows (Figure 10b). It is not obvious why fine sediment transport (which comprises roughly two-thirds of the total sediment transport) would decrease with increasing bed gradient at high discharges, when coarse transport rates at high discharges are approximately the same in the steep and flat reaches. This result is even more puzzling in view of the fact that at low discharges, total transport rates are apparently higher in the steep reach than in the flat reach.

These inconsistencies could reflect real transport behavior, but might also arise from measurement uncertainties in the two different measurement systems, complicating any direct comparison between Q_b *flat* and Q_b *steep*. On the low-gradient reach, the bed load trap sampling times (up to 1 h at low flows) might still be too short to represent the intermittent bed load transport described above. It is also possible that the bed load trap measurements on the flat reach were not representative of the entire period of record for the steep reach (2009–2015).

In the steep reach, uncertainties in the transport rates are strongly related to the quality of the geophone calibration. The calibration periods span the full range of flows and transport rates observed over the entire time series (2009–2015). In addition, the r^2 values of the calibration equations indicate strong relationships between the measured bed load volumes or weights and geophone impulses. Nonetheless, the apparent decrease in fine sediment transport rates between the flat and steep reaches during high-discharge periods (when coarse sediment transport rates are comparable between the two reaches; see Figure 10), might indicate that the geophone measurement system is insensitive to high transport rates of fine sediment. The minimum grain size that can be detected by the sensors is about 20 mm [*Rickenmann and McArdell*, 2007]. However, this grain size threshold increases, and generally the probability to register passing stones decreases, with increasing flow velocities [*Wyss et al*., 2016b]. Due to the geometry of the water intake and the geophone array, velocities up to about 3 m s^{-1} are expected during high discharges at the Riedbach; such high velocities may affect the detection capabilities of the geophone system. Similarly, as has been observed for the Erlenbach [*Wyss et al*., 2016c], it is possible that bed load transport rates are generally

underestimated at high discharges (and that this underestimation is most pronounced for smaller grain sizes), thus explaining the difference between Q_b *flat* versus Q_b *steep*.

The two bed load measurement systems presented here are believed to measure transport rates and annual loads at the right order of magnitude in both reaches, despite their measurement uncertainties and their different principles of operation. Thus if these measurements are even approximately correct, we can infer that bed load transport rates do not increase greatly with bed gradient in this study reach, as both intuition and common bed load transport equations would predict (Table 3, ID 4). The relative constancy of transport rates across such a large range of bed gradients indicates that the streambed roughness, hydraulic conditions, and bed load transport rate in each reach must be adjusted to achieve approximate long-term equilibrium with the sediment supply from upstream.

The finding of small differences in bed load volumes (smaller than a factor of 4) between the flat and the steep reach is consistent with observations from an extreme flood event in 2005 in Switzerland, in which fluvial bed load transport, normalized by effective runoff, increased only slightly as bed slope increased over the range of 2–20% [*Rickenmann and Koschni*, 2010]. Bed load volumes varied from 5000 to 2,25,000 m^3 during that event, and normalizing them by the effective runoff volume resulted in mean sediment concentrations varying from about 0.3 to 3%. For the Riedbach, mean annual sediment concentrations (i.e., bed load volumes normalized by effective runoff) vary from 0.0001 to 0.005% (Table 2). These concentrations are thus about three orders of magnitude smaller than for the data of the 2005 Swiss flood, but the relative variability between sites or channel reaches is similar for both cases, with a comparable range of bed slope variation.

4.2. Bed Load Transport Predictions

One of the objectives of this study was to test whether one can accurately predict bed load transport at very steep bed gradients, using existing flow resistance and sediment transport equations developed for lower-gradient streams. It was recently shown that common flow resistance equations based on bed roughness parameters such as the D_{84} can explain reach-averaged hydraulic conditions in the steep reach at the Riedbach [*Schneider et al*., 2015a]. However, although these flow resistance equations can predict the hydraulic conditions fairly accurately, their use in total shear stress calculations typically results in overestimation of bed load transport rates by many orders of magnitude (ID4 in Table 3 shows one example; comparable results were also obtained with other transport equations). Thus, at steep slopes energy losses due to macro-roughness need to be accounted for [*Bathurst et al*., 1987; *Chiari and Rickenmann*, 2011; *Lenzi et al*., 1999; *Nitsche et al*., 2011; *Rickenmann and Recking*, 2011; *Rickenmann et al*., 2012; *Schneider et al*., 2015b; *Yager et al*., 2007, 2012a], either by decreasing the applied shear stress using a flow resistance partitioning approach, or by increasing the critical/reference shear stress. For the Riedbach, both approaches led to more realistic estimates of bed load transport (Table 3, approaches ID 1-2 versus ID3 and supporting information Table S1), in agreement with the results of *Schneider et al*. [2015b].

Low transport rates in steep mountain streams are often attributed to limitations in sediment availability on the bed and sediment supply from upstream [*Bathurst*, 2007; *Garcia*, 1999; *Laronne and Duncan*, 1992; *Laronne et al*., 2001; *Lisle and Hilton*, 1999; *Nelson et al*., 2009; *Yager et al*., 2012b]. In the case of the Riedbach, the long-term sediment supply to the steep reach is likely to be regulated by sediment delivery from the low-gradient reach, given the evident lack of significant lateral inputs, bank erosion, or long-term aggradation or degradation of the bed. One could hypothesize that the transport capacity of the steep reach greatly exceeds the upstream sediment supply, implying that transport rates should be coupled to upstream supply on both short and long time scales. Alternatively, one could hypothesize that the bed roughness and flow hydraulics (and thus the transport capacity) of the steep reach are adjusted to the long-term upstream sediment supply. Either hypothesis could explain the rough correspondence between the measured transport rates in the steep and low-gradient reaches. However, the close agreement between the predicted and observed transport rates (Figure 9) in both the steep and low-gradient reaches is inconsistent with the first hypothesis and consistent with the second.

In both reaches the predictive accuracy is lower at low flows (and thus low transport rates), but improves considerably with increasing flows (Figure 9). Fortunately, high flows are of interest for most practical purposes, as they control both flood hazards and long-term sediment budgets (e.g., the predicted and measured annual bed loads in Table 2). The general predictive accuracy (Figure 9 and Table 2) appears to be

reasonable given that the development of equation (9) was largely independent of the Riedbach data; only data from the low-gradient reach of the Riedbach was included, among a total of 14 mountain streams, in developing equation (9). This demonstrates that transport equations that have been developed at lower gradients can also give reasonable results at very steep bed gradients. This is certainly true for the transport equations considered in this study [*Schneider et al*., 2015b; *Wilcock and Crowe*, 2003], but it may also be true for similar transport equations if the hydraulics and the energy losses due to macro-roughness are adequately represented.

5. Conclusion

We studied bed load transport in a steep mountain stream whose bed gradient increases by roughly one order of magnitude over a 1 km reach, while flow discharge and width remain approximately constant. Field measurements of bed load transport rates, analyzed together with measurements of flow and bed characteristics [*Schneider et al*., 2015a], led to the following results.

1. Due to the stable and very rough bed conditions in the steep reach (S=38%), fluvial bed load transport was observed at gradients typically associated with debris flow processes.
2. Two-phase bed load transport was observed in both reaches, characterized by a break in slope in the transport-discharge relationship. The break in slope occurred at a similar critical discharge in both reaches.
3. Bed load transport rates did not increase greatly between the flat and steep reaches despite a more than 10-fold difference in bed gradient. However, due to measurement uncertainties it is unclear whether transport rates were the same, or somewhat lower, in the steep reach.
4. Fractional transport models that account for energy losses due to macro-roughness through flow resistance partitioning can predict bulk transport rates and volumes with reasonable accuracy at higher flows. At low flows, the percentage uncertainties in the predictions are generally larger. If energy losses due to macro-roughness are neglected, bed load transport rates are greatly overestimated.

In conclusion, bed load transport equations that were developed to account for flow resistance partitioning in lower-gradient mountain streams can also predict sediment transport rates with reasonable accuracy at very steep bed gradients.

Acknowledgments
This study was supported by the CCES project APUNCH of the ETH domain. We thank the Kraftwerke Mattmark AG (KWM) for supporting our research at the Riedbach. We thank K. Steiner, N. Federspiel and A. Beer for field assistance. We thank K. Bunte for providing pebble count grain size distributions and helpful discussions. We thank Vincenzo D'Agostino and two anonymous reviewers for their constructive comments that helped to improve the manuscript. The bed load transport data (supporting information Data Set S1) and channel geometry data (supporting information Data Set S2) collected in this study are available as supporting information accompanying this paper.

References

Badoux, A., N. Andres, and J. M. Turowski (2014), Damage costs due to bedload transport processes in Switzerland, *Nat. Hazards Earth Syst. Sci.*, *14*(2), 279–294, doi:10.5194/nhess-14-279-2014.

Bathurst, J. C. (2007), Effect of coarse surface layer on bed-load transport, *J. Hydraul. Eng.*, *133*(11), 1192–1205, doi:10.1061/(ASCE)0733-9429(2007)133:11(1192).

Bathurst, J. C., G. W. H., and H. H. Cao (1987), Bed load discharge equations for steep mountain rivers, in *Sediment Transport in Gravel-Bed Rivers*, edited by C. R. Thorne, J. C. Bathurst and R. D. Hey, pp. 453–477, John Wiley, New York.

Beschta, R. L. (1987), Conceptual models of sediment transport in streams, in *Sediment Transport in Gravel-Bed Rivers*, edited by C. R. Thorne, J. C. Bathurst, and R. D. Hey, pp. 387–419, John Wiley, New York.

Buffington, J. M., and D. R. Montgomery (1997), A systematic analysis of eight decades of incipient motion studies, with special reference to gravel-bedded rivers, *Water Resour. Res.*, *33*(8), 1993–2029, doi:10.1029/96WR03190.

Bunte, K., F. Rocky Mountain, and S. Range Experiment (1996), *Analyses of the Temporal Variation of Coarse Bedload Transport and its Grain Size Distribution: Squaw Creek, Montana, USA*, 123 pp., U.S. Dep. of Agric., For. Serv., Rocky Mt. For. and Range Exp. Stn., Fort Collins, Colo.

Bunte, K., S. R. Abt, J. P. Potyondy, and S. E. Ryan (2004), Measurement of coarse gravel and cobble transport using portable bedload traps, *J. Hydraul. Eng.*, *130*(9), 879–893, doi:10.1061/(ASCE)0733-9429(2004)130:9(879).

Bunte, K., S. R. Abt, J. P. Potyondy, and K. W. Swingle (2009), Comparison of Three Pebble Count Protocols (EMAP, PIBO, and SFT) in two mountain gravel-bed streams, *J. Am. Water Resour. Assoc.*, *45*(5), 1209–1227, doi:10.1111/j.1752-1688.2009.00355.x.

Bunte, K., S. R. Abt, K. W. Swingle, D. A. Cenderelli, and J. M. Schneider (2013), Critical Shields values in coarse-bedded steep streams, *Water Resour. Res.*, *49*, 7427–7447, doi:10.1002/2012WR012672.

Camenen, B. (2012), Discussion of "Understanding the influence of slope on the threshold of coarse grain motion: Revisiting critical stream power" by C. Parker, N.J. Clifford, and C.R. Thorne Geomorphology, Volume 126, March 2011, Pages 51-65, *Geomorphology*, *139–140*, 34–38, doi:10.1016/j.geomorph.2011.10.033.

Chiari, M., and D. Rickenmann (2011), Back-calculation of bedload transport in steep channels with a numerical model, *Earth Surf. Processes Landforms*, *36*(6), 805–815, doi:10.1002/esp.2108.

Chiari, M., K. Friedl, and D. Rickenmann (2010), A one-dimensional bedload transport model for steep slopes, *J. Hydraul. Res.*, *48*(2), 152–160, doi:10.1080/00221681003704087.

Church, M., M. A. Hassan, and J. F. Wolcott (1998), Stabilizing self-organized structures in gravel-bed stream channels: Field and experimental observations, *Water Resour. Res.*, *34*(11), 3169–3179.

Egashira, S., and K. Ashida (1991), Flow resistance and sediment transportation in streams with step-pool bed morphology, in *Fluvial Hydraulics of Mountain Regions*, edited by A. Armanini and G. Silvio, pp. 45–58, Springer, Berlin.
Fehr, R. (1987), A method for sampling very coarse sediments in order to reduce scale effects in movable bed models, in *Proceedings of IAHR Symposium on Scale Effects in Modelling Sediment Transport Phenomena*, 383–397, Toronto, Canada.
Ferguson, R. I. (2007), Flow resistance equations for gravel- and boulder-bed streams, *Water Resour. Res.*, *43*, W05427, doi:10.1029/2006WR005422.
Ferguson, R. I. (2012), River channel slope, flow resistance, and gravel entrainment thresholds, *Water Resour. Res.*, *48*, W05517, doi:10.1029/2011WR010850.
Garcia, C. (1999), Variable source areas of bedload in a gravel-bed stream, *J. Sediment. Res.*, *69*, 27–31.
Knighton, A. D. (1980), Longitudinal changes in size and sorting of stream- bed material in four English rivers, *Geol. Soc. Am. Bull.*, *91*(1 pt I), 55–62.
Lajeunesse, E., L. Malverti, and F. Charru (2010), Bed load transport in turbulent flow at the grain scale: Experiments and modeling, *J. Geophys. Res. Earth Surf.*, *115*, F04001, doi:10.1029/2009JF001628.
Lamb, M. P., W. E. Dietrich, and J. G. Venditti (2008), Is the critical Shields stress for incipient sediment motion dependent on channel-bed slope?, *J. Geophys. Res.*, *113*, F02008, doi:10.1029/2007JF000831.
Laronne, J. B., and M. J. Duncan (1992), Bedload transport paths and gravel bar formation, in *Dynamics of Gravel-Bed Rivers*, edited by P. Billi et al., pp. 177–202, John Wiley, Chichester, U. K.
Laronne, J. B., C. Garcia, and I. Reid (2001), Mobility of patch sediment in gravel bed streams: Patch character and its implications for bedload, in *Gravel-Bed Rivers V*, edited by M. P. Mosley, pp. 249–290, N. Z. Hydrol. Soc. Inc., Wellington.
Lenzi, M. A., V. D'Agostino, and P. Billi (1999), Bedload transport in the instrumented catchment of the Rio Cordon Part I: Analysis of bedload records, conditions and threshold of bedload entrainment, *Catena*, *36*(3), 171–190, doi:10.1016/s0341-8162(99)00016-8.
Lisle, T. E., and S. Hilton (1999), Fine bed material in pools of natural gravel bed channels, *Water Resour. Res.*, *35*(4), 1291–1304, doi:10.1029/1998WR900088.
Ma, H., J. Heyman, X. Fu, F. Mettra, C. Ancey, and G. Parker (2014), Bed load transport over a broad range of timescales: Determination of three regimes of fluctuations, *J. Geophys. Res. Earth Surf.*, *119*, 2653–2673, doi:10.1002/2014JF003308.
Mao, L., A. Dell'Agnese, C. Huincache, D. Penna, M. Engel, G. Niedrist, and F. Comiti (2014), Bedload hysteresis in a glacier-fed mountain river, *Earth Surf. Processes Landforms*, *39*(7), 964–976, doi:10.1002/esp.3563.
Meyer-Peter, E., and R. Müller (1948), Formulas for bedload transport, in *Proceedings of the 2nd Meeting of the International Association for Hydraulic Structures Research*, pp. 39–64, Int. Assoc. for Hydraul. Struct. Res., Stockholm.
Millar, R. G. (1999), Grain and form resistance in gravel-bed rivers, *J. Hydraul. Res.*, *37*(3), 303–312.
Millar, R. G., and M. Quick (1994), Flow resistance of high-gradient gravel channels, in *Hydraulic Engineering (1994)*, edited by G. V. Cotroneo and R. R. Rumer, pp. 717–721, Am. Soc. Civ. of Eng., New York.
Montgomery, D. R., and J. M. Buffington (1997), Channel-reach morphology in mountain drainage basins, *Geol. Soc. Am. Bull.*, *109*(5), 596–611.
Moog, D. B., and P. J. Whiting (1998), Annual hysteresis in bed load rating curves, *Water Resour. Res.*, *34*(9), 2393–2399, doi:10.1029/98WR01658.
Mueller, E. R., and J. Pitlick (2013), Sediment supply and channel morphology in mountain river systems: 1. Relative importance of lithology, topography, and climate, *J. Geophys. Res. Earth Surf.*, *118*, 2325–2342, doi:10.1002/2013JF002843.
Mueller, E. R., J. Pitlick, and J. M. Nelson (2005), Variation in the reference shields stress for bed load transport in gravel-bed streams and rivers, *Water Resour. Res.*, *41*, W04006, doi:10.1029/2004WR003692.
Nelson, P. A., J. G. Venditti, W. E. Dietrich, J. W. Kirchner, H. Ikeda, F. Iseya, and L. S. Sklar (2009), Response of bed surface patchiness to reductions in sediment supply, *J. Geophys. Res.*, *114*, F02005, doi:10.1029/2008JF001144.
Nitsche, M., D. Rickenmann, J. M. Turowski, A. Badoux, and J. W. Kirchner (2011), Evaluation of bedload transport predictions using flow resistance equations to account for macro-roughness in steep mountain streams, *Water Resour. Res.*, *47*, W08513, doi:10.1029/2011WR010645.
Pagliara, S., and P. Chiavaccini (2006), Flow resistance of rock chutes with protruding boulders, *J. Hydraul. Eng.*, *132*(6), 545–552.
Prancevic, J. P., and M. P. Lamb (2015), Unraveling bed slope from relative roughness in initial sediment motion, *J. Geophys. Res. Earth Surf.*, *120*, 474–489, doi:10.1002/2014JF003323.
Prancevic, J. P., M. P. Lamb, and B. M. Fuller (2014), Incipient sediment motion across the river to debris-flow transition, *Geology*, *42*(3), 191–194, doi:10.1130/g34927.1.
Recking, A. (2009), Theoretical development on the effects of changing flow hydraulics on incipient bed load motion, *Water Resour. Res.*, *45*, W04401, doi:10.1029/2008WR006826.
Recking, A. (2010), A comparison between flume and field bed load transport data and consequences for surface-based bed load transport prediction, *Water Resour. Res.*, *46*. W03518, doi:10.1029/2009WR008007.
Recking, A. (2012), Influence of sediment supply on mountain streams bedload transport, *Geomorphology*, *175-176*, 139–150.
Recking, A., G. Piton, D. Vazquez-Tarrio, and G. Parker (2015), Quantifying the morphological print of bedload transport, *Earth Surf. Processes Landforms*, *41*, 809–822, doi:10.1002/esp.3869.
Rice, S., and M. Church (1998), Grain size along two gravel-bed rivers: Statistical variation, spatial pattern and sedimentary links, *Earth Surf. Processes Landforms*, *23*(4), 345–363.
Rickenmann, D. (2012), Alluvial steep channels: Flow resistance, bedload transport prediction, and transition to debris flows, in *Gravel-Bed Rivers: Processes, Tools, Environments* (2012), edited by M. Church, P. M. Biron, and A. G. Roy, pp. 386–397, John Wiley, Chichester, U. K.
Rickenmann, D., and A. Koschni (2010), Sediment loads due to fluvial transport and debris flows during the 2005 flood events in Switzerland, *Hydrol. Processes*, *24*(8), 993–1007.
Rickenmann, D., and B. W. McArdell (2007), Continuous measurement of sediment transport in the Erlenbach stream using piezoelectric bedload impact sensors, *Earth Surf. Processes Landforms*, *32*(9), 1362–1378, doi:10.1002/esp.1478.
Rickenmann, D., and A. Recking (2011), Evaluation of flow resistance in gravel-bed rivers through a large field data set, *Water Resour. Res.*, *47*, W07538, doi:10.1029/2010WR009793.
Rickenmann, D., J. M. Turowski, B. Fritschi, A. Klaiber, and A. Ludwig (2012), Bedload transport measurements at the Erlenbach stream with geophones and automated basket samplers, *Earth Surf. Processes Landforms*, *37*(9), 1000–1011, doi:10.1002/esp.3225.
Rickenmann, D., et al. (2014), Bedload transport measurements with impact plate geophones: Comparison of sensor calibration in different gravel-bed streams, *Earth Surf. Processes Landforms*, *39*(7), 928–942, doi:10.1002/esp.3499.
Ryan, S. E., L. S. Porth, and C. A. Troendle (2005), Coarse sediment transport in mountain streams in Colorado and Wyoming, USA, *Earth Surf. Processes Landforms*, *30*(3), 269–288, doi:10.1002/esp.1128.

Schneider, J. M., J. M. Turowski, D. Rickenmann, R. Hegglin, S. Arrigo, L. Mao, and J. W. Kirchner (2014), Scaling relationships between bed-load volumes, transport distances and stream power in steep mountain channels, *J. Geophys. Res. Earth Surf.*, *119*, 533–549, doi:10.1002/2013JF002874.

Schneider, J. M., D. Rickenmann, J. M. Turowski, and J. W. Kirchner (2015a), Self-adjustment of stream bed roughness and flow velocity in a steep mountain channel, *Water Resour. Res.*, *51*, 7838–7859, doi:10.1002/2015WR016934.

Schneider, J. M., D. Rickenmann, J. M. Turowski, K. Bunte, and J. W. Kirchner (2015b), Applicability of bed load transport models for mixed-size sediments in steep streams considering macro-roughness, *Water Resour. Res.*, *51*, 5260–5283, doi:10.1002/2014WR016417.

Schumm, S. A. (1977), *The Fluvial System*, 338 pp., John Wiley, Chichester and New York.

Shields, A. (1936), Application of similarity principles and turbulence research to bed-load movement. In: W. P. Ott and J. C. Uchelen (translators), Mitt. Preuss. Versuchsanst., Berlin. Wasserbau Schiffbau, *Rep*. 167, 43 pp., Calif. Inst. of Technol., Pasadena.

Shvidchenko, A. B., G. Pender, and T. B. Hoey (2001), Critical shear stress for incipient motion of sand/gravel streambeds, *Water Resour. Res.*, *37*(8), 2273–2283, doi:10.1029/2000WR000036.

Turowski, J. M., and D. Rickenmann (2011), Measuring the statistics of bed-load transport using indirect sensors, *J. Hydraul. Eng.*, *137*(1), 116–121, doi:10.1061/(ASCE)hy.1943-7900.0000277.

Turowski, J. M., A. Badoux, and D. Rickenmann (2011), Start and end of bedload transport in gravel-bed streams, *Geophys. Res. Lett.*, *38*, L04401, doi:10.1029/2010GL046558.

VAW/ETHZ, and EKK/SCNAT (2015), Gletscherberichte (1881-2016). "Die Gletscher der Schweizer Alpen", Jahrbücher der Expertenkommission für Kryosphärenmessnetze der Akademie der Naturwissenschaften Schweiz (SCNAT), report 1–134, Versuchsanst. für Wasserbau, Hydrol. und Glaziologie (VAW), Zurich. [Available at http://glaciology.ethz.ch/swiss-glaciers/.]

Warburton, J. (1992), Observations of bed load transport and channel bed changes in a proglacial mountain stream, *Arct. Alp. Res.*, *24*(3), 195–203.

Whittaker, J. G., W. E. Hickman, and R. N. Croad (1988), Riverbed stabilisation with placed blocks, report 3-88/3, Hydraul. Sect., Cent. Lab., Works Corp., Lower Hutt, New Zealand. [Available at http://books.google.ch/books?id=M0mBMQAACAAJ.]

Wilcock, P. R., and J. C. Crowe (2003), Surface-based transport model for mixed-size sediment, *J. Hydraul. Eng.*, *129*(2), 120–128, doi:10.1061/(ASCE)0733-9429(2003)129:2(120).

Wilcock, P. R., J. Pitlick, and Y. Cui (2009), Sediment transport primer: Estimating bed-material transport in gravel-bed rivers, Gen. Tech. Rep. RMRS-GTR-226, Fort Collins, CO: U.S. Department of Agriculture, Forest Service, Rocky Mountain Research Station, 78 pp., Fort Collins, Colo.

Wohl, E. (2000), *Mountain Rivers*, AGU, Washington, D. C.

Wolman, G. M. (1954), A method of sampling coarse river-bed material, *Eos Trans. AGU*, *35*(6), 951–956.

Wyss, C. R., D. Rickenmann, B. Fritschi, J. Turowski, V. Weitbrecht, and R. Boes (2016a), Measuring bed load transport rates by grain-size fraction using the Swiss Plate Geophone Signal at the Erlenbach, *J. Hydraul. Eng.*, *142*(5), 04016003, doi:10.1061/(ASCE)HY.1943-7900.0001090.

Wyss, C. R., D. Rickenman, B. Fritschi, J. M. Turowski, V. Weitbrecht, and R. Boes (2016b), Laboratory flume calibration of the Swiss plate geophone bedload monitoring system. Part I: Impulse counts and particle size identification, *Water Resour. Res.*, *52*, 7744–7759, doi:10.1002/2015WR018555.

Wyss, C. R., D. Rickenmann, B. Fritschi, J. M. Turowski, V. Weitbrecht, E. Travaglini, E. Bardou, and R. M. Boes (2016c), Laboratory flume experiments with the Swiss plate geophone bedload monitoring system. Part II: Application to field sites with direct bedload samples, *Water Resour. Res.*, *52*, 7760–7778, doi:10.1002/2016WR019283.

Yager, E. M., J. W. Kirchner, and W. E. Dietrich (2007), Calculating bed load transport in steep boulder bed channels, *Water Resour. Res.*, *43*, W07418, doi:10.1029/2006WR005432.

Yager, E. M., W. E. Dietrich, J. W. Kirchner, and B. W. McArdell (2012a), Prediction of sediment transport in step-pool channels, *Water Resour. Res.*, *48*, W01541, doi:10.1029/2011WR010829.

Yager, E. M., W. E. Dietrich, J. W. Kirchner, and B. W. McArdell (2012b), Patch dynamics and stability in steep, rough streams, *J. Geophys. Res.*, *117*, F02010, doi:10.1029/2011JF002253.

Yang, C. T. (1996), *Sediment Transport: Theory and Practice*, McGraw-Hill, New York.